Calibration of Photomultiplier Arrays

F. Neves[4,1], V. Chepel[4], D. Yu. Akimov[5], H. M. Araújo[1,2], E. J. Barnes[3], V. A. Belov[5], A. A. Burenkov[5], B. Currie[1], B. Edwards[1,2], C. Ghag[3], M. Horn[1], A. J. Hughes[2], G. E. Kalmus[2], A. S. Kobyakin[5], A. G. Kovalenko[5], V. N. Lebedenko[5], A. Lindote[4], M. I. Lopes[4], R. Lüscher[3], K. Lyons[1], P. Majewski[2], A. StJ. Murphy[3], J. Pinto da Cunha[4], R. Preece[3], J. J. Quenby[1], P. R. Scovell[3], C. Silva[4], V. N. Solovov[4], N. J. T. Smith[2], P. F. Smith[2], V. N. Stekhanov[5], T. J. Sumner[1], C. Thorne[1], R. J. Walker[1]

[1]Blackett Laboratory, Imperial College London, UK
[2]Particle Physics Department, Rutherford Appleton Laboratory, Chilton, UK
[3]School of Physics and Astronomy, University of Edinburgh, UK
[4]LIP–Coimbra & Department of Physics of the University of Coimbra, Portugal
[5]Institute for Theoretical and Experimental Physics, Moscow, Russia

Abstract. A method is described that allows calibration and assessment of the linearity of response of an array of photomultiplier tubes. The method does not require knowledge of the photomultiplier single photoelectron response model and uses science data directly, thus eliminating the need for dedicated data sets. In this manner all photomultiplier working conditions (e.g. temperature, external fields, etc) are exactly matched between calibration and science acquisitions. This is of particular importance in low background experiments such as ZEPLIN-III, where methods involving the use of external light sources for calibration are severely constrained.

Keywords: photomultipliers, calibration, linearity, ZEPLIN-III

1. Introduction

Traditional procedures to characterize the response of a photomultiplier tube (PMT) rely, typically, on the use of calibration light sources and dedicated trigger setups. However, in some experiments, such as the ZEPLIN-III WIMP search [1, 2, 3], the use and positioning of these light sources is severely constrained both by the low radioactivity background requirement and by the use of VUV-rated components. Also, it is known that the response of a PMT depends on its working conditions, namely, external fields and temperature. In its already long history there have been several attempts to model the response function of a PMT ($\mathscr{R}$). Nevertheless, a general solution which covers different working conditions and different types of PMT is still missing.

Based on experimental data obtained using Ni and Be dynodes, Wright stated that the number of secondary electrons ejected per primary electron is described by a Poisson distribution (P) [4]. The effect of non-uniform photocathode and dynode surfaces or inter-stage collection efficiencies (focusing optics) is the variation of the mean of the distribution (η) from one primary electron to another, thus increasing the variance of the PMT response function ($\sigma_{\mathscr{R}}$). The calculations presented did not allow to conclude on the shape of this response function, but only to infer that, being the effect of non-uniformities negligible, the dominant statistics would be *gaussian* for a sufficiently large number of photoelectrons. Nevertheless, Breitenberger [5] reported that the electron multiplication variance measured using activated BaO + SrO dynodes is in fact larger than calculated when assuming a *poissonian* secondary emission process $P(n, \eta)$. Based on the same assumption, Lombard *et al.* [6] derived the pulse height spectrum for cascades starting with single photoelectrons. The authors remarked that their results were inconsistent with observed data, thus rejecting the hypothesis of the Poisson distribution (P) being a good descriptor for the PMT electron multiplication process. In spite of this conclusion, other authors[7, 8, 9] consistently reported measurements which did agree with the calculations by Lombard *et al.* [6] and attribute the discrepant results of other work to noise in their experimental setup [9]. Using an *exponential* distribution to describe the electron multiplication at the dynodes, Prescott *et al.* [10] obtained good agreement between calculated and measured spectra for some specific types of PMT.

Baldwin *et al.* [11] suggested that the inconsistent results mentioned above could be explained in terms of the microscopic characteristics of the dynodes used. In fact, the random orientations of the polycrystals in the Ag + MgO dynodes used by Lombard *et al.* [6] are consistent with a variation of the mean number of secondary electrons (η) produced by primaries hitting different regions [4]. On the other hand, the Sb + CsO dynodes used by Tusting *et al.* [9] consist of a more uniform thin layer of adsorbed material, which may account for a more constant η across the surface [11]. A possible conclusion from these evidences [12] is that one can assume that at each PMT stage the electron multiplication process follows indeed a Poisson distribution (P) given dynodes with uniform emission properties [4, 5, 6].

In order to generalize the description of the fluctuations in the secondary electron emission process, Prescott [13] had proposed the use of the *Polya* distribution which contains the *Furry* (*exponential*) and Poisson distributions as special cases. The *Polya* distribution is also used in the description of cosmic-ray fluctuations and of charge multiplication in proportional counters [13]. For a PMT, the *Polya* describes the multiplication process when the number of secondary electrons follows a Poisson

distribution (P) with η varying across the dynode surface in a manner described by the *Laplace* distribution [13]. Once again it was verified experimentally that the *Polya* distribution can only model the response for a limited number of PMTs [13, 14].

More recent work involved a Monte Carlo simulation of dynode statistics to assess the overall PMT response resolution[14]. In spite of predicting accurately the resolution for a range of PMTs [14], the method demands the single electron response (SER) to be measured experimentally. The issue is again that measuring the SER at the working conditions (e.g. temperature, external field) of PMTs installed in some experimental setups may present an insurmountable challenge.

In the present work we propose an application of an existing method to calibrate a PMT which does not demand the knowledge of its SER model. Instead, the method relies only on the statistical description of the light pulses arriving at the PMT photocathode. This fact eliminates the need for dedicated data sets acquired using calibration light sources, but allows for the use of the light pulses produced in the sensitive volume of a detector during its science exposure. In this manner, all the working conditions of a PMT (external fields, temperature, light intensity, trigger, signal amplification and conditioning) are perfectly matched between the calibration procedure and the science data. One more significant advantage is that it eliminates any difficulties posed by setting up the calibration light(s) in the context of a particular experiment. Finally, one must emphasize that the proposed method of calibration is more suitable for a detector having an array of PMTs instead of a single one. This is related to the fact that an array permits the implementation of some sort of position reconstruction, thus allowing the effect of differences in the light collection efficiency across the active volume of the detector to be minimised.

2. Setup and Data Processing

ZEPLIN-III is a two-phase (liquid/gas) xenon time projection chamber designed to search for dark matter WIMPs [1, 2, 3]. The active volume contains ≈ 12 kg of liquid xenon above a compact hexagonal array of 31 2-inch PMTs (ETL D730/9829Q). The PMTs are immersed directly in the liquid at a temperature of ≈ -105 ^{o}C and record both the rapid scintillation signal (S1) and a delayed second signal (S2) produced by proportional electroluminescence in the gas phase from charge drifted out of the liquid [1]. The electric field in the active xenon volume is defined by a cathode wire grid 36 mm below the liquid surface and an anode plate 4 mm above the surface in the gas phase. These two electrodes define a drift field in the liquid of 3.9 kV/cm and an electroluminescence field in the gas of 7.8 kV/cm. A second wire grid is located 5 mm below the cathode grid just above the PMT array. This grid defines a reverse field region which suppresses the collection of ionization charge for events just above the array and helps to isolate the PMTs input optics from the external high electric field.

The PMT signals are digitized at 2 ns sampling over a time segment of ± 18 μs either side of the trigger point. Each PMT signal is fed into two 8-bit digitizers (ACQIRIS DC265) with a $\times 10$ gain difference between them provided by fast amplifiers (Phillips Scientific 770), to obtain both high and low sensitivity readout covering a wide dynamic range. The PMT array is operated from a common HV supply with attenuators (Phillips Scientific 804) used to normalize their individual gains. The trigger is created from the shaped sum signal of all the PMTs.

The raw data are processed and reduced by a purpose developed software tool (ZE3RA), which finds candidate pulses in individual waveforms by searching for

signal excursions over a defined threshold (V_{thr}) [3]. Subsequent waveform processing includes resolving adjacent/overlapping pulses, grouping of statistically consistent structures (e.g. scintillation tails) and coincidence analysis of occurrences in different channels. By design, ZE3RA outputs only amplitude, area and timing parameters and does not ascribe any physical meaning to pulses. This task is left to an independent software tool which processes the original parameters assigning a physical meaning to the reduced data. This assignment is made according to a well defined set of rules, e.g. primary scintillation signals (S1) are fast and must precede wider electroluminescence signals (S2).

Using S2 pulses from a ^{57}Co source located above the instrument, an iterative procedure was used to normalize the measured response from each PMT (i.e. 'flat-field' the array) [15]. The procedure is based on fitting to each channel a common cylindrical response profile extending away from the vertical PMT axis and does not depend on the characterization of the individual PMT response. Position reconstruction in the horizontal plane was then achieved by using the converged response profiles in a simultaneous least-squares minimization to all channels [15]. The vertical position is obtained by measuring the time difference between S1 and S2 signals corresponding to the electron drift time in the liquid.

3. Methodology

Arising from the fact that photons follow Bose-Einstein statistics, the Poisson distribution is a good approximation to the number of photons arriving at the photocathode within a defined time window [16, 17]. As the photoemission process follows the binomial distribution (with the quantum efficiency ϵ quantifying the probability of one photon producing one photoelectron), it has been shown that the number of photoelectrons n produced in the photocathode also follows a Poisson distribution [16]

$$P(\mu, n) = \frac{\mu^n e^{-\mu}}{n!} \ , \tag{1}$$

where μ is the mean number of photoelectrons. The value of μ has a simple relation to the mean number of incident photons of μ/ϵ. Reworking Eq. 1 one obtains [18]

$$\frac{P(\mu, 0)}{\sum_{k=0}^{+\infty} P(\mu, k)} = \frac{N_0}{N} \Longrightarrow \mu = -ln\left(N_0/N\right) \ , \tag{2}$$

where N stands for the total number of opened time windows (incident light pulses) and N_0 for the number of times there were *no* photoelectrons produced in the photocathode.

In a general setup, the signals from a PMT are fed into some sort of acquisition system (DAQ) allowing ultimately measurement of the number of electrons arriving at the anode. This implies that the assertion of the *null* photoelectron signal ($P(\mu, 0)$) must be made against a measure of the noise intrinsic to the DAQ system used. In ZEPLIN-III the noise distribution was parametrized using the same waveforms containing the actual PMT signals [3]. To avoid any bias due to the occurrence of a transient or small signal, the parametrization method relies on a consistency check of the noise distribution variance during a sufficiently large time window. For that purpose, the DAQ *pre*-trigger region is divided into $i = 1..M_0$ consecutive regions containing m samples each. For each of these regions, the variance $\left\{\sigma_i^2,\, i = 1..M_0\right\}$

of the signal amplitude distribution is calculated and the F-distribution probability function (Q) is used to check if they are statistically consistent:

$$Q = \frac{\Gamma(\frac{\nu_a}{2}+\frac{\nu_b}{2})}{\Gamma(\frac{\nu_a}{2})\Gamma(\frac{\nu_b}{2})}\int_0^{\frac{\nu_b/2}{\nu_b/2+F\nu_a/2}} t^{\frac{\nu_a}{2}-1}(1-t)^{\frac{\nu_b}{2}-1}dt \ , \tag{3}$$

where

$$\begin{cases} \nu_a = m_i - 1,\ \nu_b = m_{i+1} - 1, & \sigma_i > \sigma_{i+1} \\ \nu_a = m_{i+1} - 1,\ \nu_b = m_i - 1, & \sigma_i \leq \sigma_{i+1} \end{cases} \ ,$$

and

$$\begin{cases} F = \sigma_i^2/\sigma_{i+1}^2, & \sigma_i > \sigma_{i+1} \\ F = \sigma_{i+1}^2/\sigma_i^2, & \sigma_i \leq \sigma_{i+1} \end{cases} \ .$$

Q is therefore the significance level at which that hypotheses ($\sigma_i^2 \equiv \sigma_{i+1}^2$, $i = 1..M_0$) can be rejected [19]. In the present work the values of $m = 25$ (50 ns) and $Q = 0.0001$ were used. The maximum length of the total sampled waveform was 2 μs ($M_0 = 40$). The noise characterizing each waveform is then defined as

$$\sigma = \langle \sigma_i \rangle \ , \ i = 1..M \ , \tag{4}$$

for those M regions satisfying Eq. 3. Waveforms for which $M < 20$ (1 μs) were not considered for the analysis. Fig. 1 shows the distribution of σ values for the central PMT in the ZEPLIN-III array. It can be seen that there are two peaks both having a *gaussian*-like profile. The peak corresponding to higher values of σ is due to the occurrence of an external frequency pickup which can be identified by simple visual inspection of the waveforms. With the described analysis this presents no problem as the noise is parametrized independently for each of the individual waveforms.

Setting the software amplitude threshold (V_{thr}) to a certain level (k) above the waveform noise (σ)

$$V_{thr} = k\sigma \ , \tag{5}$$

and selecting pulses which are predicted to have the same average number of photons arriving at the photocathode of a particular PMT, one can calculate μ (Eq. 2) just by defining N as the number of selected pulses and N_0 as the number of those having an amplitude $V < V_{thr}$. This definition is the core of the calibration method described here as it sets the conditions for observing *no* photoelectrons ($n = 0$) or any number of photoelectrons ($n \geq 1$) produced at the photocathode. Repeating the procedure for all PMTs and a range of expected signal allows comparison of the average PMT response in each iteration against the expected Poisson mean (μ). When selecting pulses, care must be taken to ensure that $N - N_o \ggg N_{noise}$, where N_{noise} is the expected number of occurrences leaking from the noise distribution above V_{thr}. For $k = 3$ (Eq. 5) and a normally distributed noise, values of $\mu \gtrsim 0.1$ should be used ($N \gtrsim 1.13N_0$). With this assumption the dominant error is the statistical uncertainty associated with the Bernoulli trial of observing either $n = 0$ or $n \geq 1$ photoelectrons from each incident light pulse. Defining B as the probability of $n = 0$ at a given V_{thr}, the respective variance from the Bernoulli distribution is expressed as $\sigma_{n=0}^2 = B(1 - B)$. Applying the central limit theorem to a set of N independent trials (or incident light pulses),

the variance of the random variable N_0 counting the number of $n = 0$ occurrences can be written as [18]

$$\sigma^2_{N_0} \cong N\sigma^2_{n=0} = NB(1-B) \ . \tag{6}$$

Propagating this result into Eq. 2 we obtain

$$\sigma^2_\mu \cong \frac{1-B}{NB} \ . \tag{7}$$

Considering that N_0 is drawn from a binomial distribution with mean NB then, taking the same validity constrains as for Eq. 6, $N_0 \cong NB$; feeding this into Eq. 7 results in

$$\sigma^2_\mu \cong \frac{1}{N_0} - \frac{1}{N} \ . \tag{8}$$

Combining Eq. 2 and Eq. 8 one can derive the number of incident light pulses (N) needed to keep the relative error (δ) below a required value

$$\frac{\sigma^2_\mu}{\mu^2} < \delta^2 \Longrightarrow N > \frac{1}{\mu^2\delta^2}\left(e^\mu - 1\right) \ . \tag{9}$$

Whenever a limited statistics (N) is available, Eq. 9 can also be used to determine the interval for which μ can be obtained within a certain accuracy (δ).

Assuming that the photoelectron emission at the photocathode and the secondary electron multiplication at the dynodes are independent, the relative variance of the PMT response function ($\mathscr{R}$) for $V > V_{thr}$ ($n > 0$) can be obtained by adding the relative variances from the distributions describing both processes

$$\left(\frac{\sigma_{\mathscr{R}}}{\langle\mathscr{R}\rangle}\right)^2_{V>V_{thr}} = \left(\frac{\sigma_{n>0}}{\mu_{n>0}}\right)^2 + \frac{1}{\mu_{n>0}}\left(\frac{\sigma_{\mathscr{R}}}{\langle\mathscr{R}\rangle}\right)^2_{SER} \ , \tag{10}$$

where

$$\mu_{n>0} = \frac{\sum_{n=1}^{\infty} P(\mu,n)n}{\sum_{n=1}^{\infty} P(\mu,n)} = \frac{\mu}{1-e^{-\mu}} \, , \tag{11}$$

and

$$\sigma^2_{n>0} = \frac{\sum_{n=1}^{\infty} P(\mu,n)(n-\mu_{n>0})^2}{\sum_{n=1}^{\infty} P(\mu,n)} \, , \tag{12}$$

represent, respectively, the mean ($\mu_{n>0}$) and the variance ($\sigma^2_{n>0}$) of the photoelectron distribution (Eq. 1) for $n > 0$. Using Eq. 11 and Eq. 12, the relative variance contribution from the photoelectron emission process can be written as

$$\left(\frac{\sigma_{n>0}}{\mu_{n>0}}\right)^2 = \frac{1-e^{-\mu}-\mu e^{-\mu}}{\mu} \, . \tag{13}$$

The contribution from the electron multiplication process in Eq. 10 is derived simply by applying the central limit theorem to the PMT SER relative variance ($(\sigma_{\mathscr{R}}/\langle\mathscr{R}\rangle)^2$) when a set of $\mu_{n>0}$ photoelectrons are produced at the photocathode.

4. Results

The following results were obtained using three different data sets, which are described in detail in Ref. [3]:

(i) low-energy Compton-scattered γ events from a ^{137}Cs calibration source positioned above the detector;

(ii) low-energy events from a Am-Be neutron source positioned off-center, above the detector;

(iii) 847 kg.days of WIMP-search data acquired over 83 days of continuous stable operation.

The raw data were processed using a software threshold of $V_{thr} = 3\sigma$ (Eq. 5). The PMT calibration was performed using the fast S1 (primary scintillation) signals. The expected number of S1 photons arriving at each PMT photocathode for individual events is derived from the $3D$ position reconstruction algorithm used. The μ value is calculated for each PMT channel and for each range of number of photons by applying the method described in Sec. 3. For each range the corresponding PMT response was calculated averaging the area (A) of the selected pulses. The resulting $A(\mu)$ distributions for the different PMTs and data sets were then fitted using a linear function. The errors associated with the calculation of A are insignificant and therefore were not considered in the fitting procedure. The results obtained show that there is a good linearity of response for all the PMTs in the $0.2 \lesssim \mu \lesssim 4$ interval ($\delta \lesssim 5\%$, Eq. 9). The slope on the fitted lines is an estimator for the mean response to the PMTs for single photoelectron signals ($\langle \mathscr{R} \rangle_{SER}$). Both the distributions of μ as a function of A and the corresponding fits for each of the data sets are shown in Figs. 2-4 for three different PMTs. These are representative of the results found for the whole set of 31 PMTs.

The widths of the single electron response ($(\sigma_{\mathscr{R}})_{SER}$) for all the PMTs were determined feeding the estimated values of $\langle \mathscr{R} \rangle_{SER}$ into Eq. 10. For each value of μ, the relative variance of the PMT response was calculated using the mean ($(\langle \mathscr{R} \rangle \equiv A)_{V>V_{thr}}$) and *root mean square* ($(\sigma_{\mathscr{R}} \equiv rms)_{V>V_{thr}}$) from the corresponding area distribution of pulses above the threshold ($V > V_{thr}$, Eq. 5). The errors concerning the calculation of $A_{V>V_{thr}}$ and $rms_{V>V_{thr}}$ are insignificant and were not considered. The obtained values of $(\sigma_{\mathscr{R}})_{SER}$ for the ^{137}Cs, Am-Be and WIMP-search data sets are shown in Fig. 5 for the same PMT also represented in Fig. 3.

The array-averaged mean value of the PMT SER ($\langle \langle \mathscr{R} \rangle_{SER} \rangle$) was found to be respectively $\approx 5.9\%$ and $\approx 10.3\%$ lower for the ^{137}Cs and Am-Be calibration data sets with respect to the WIMP-search data set. Simultaneously, the array average of the relative SER width ($\langle (\sigma_{\mathscr{R}} / \langle \mathscr{R} \rangle)_{SER} \rangle$) degrade by $\approx 2.8\%$ and $\approx 8.1\%$ for the ^{137}Cs and Am-Be data sets when compared to the WIMP-search data set. It should be noted that these computations assume a uniform position distribution of the S1 signals across the entire detector active volume. This assumption is not exact, especially for the Am-Be data set, due to the position of the source. Nevertheless, the observed differences on the mean PMT responses for the different data sets are attributed to the increase in the resistivity of the bialkali photocathodes at low temperatures [20, 21]. To cope

with this well known effect, the PMTs used have a set of metal tracks deposited under the photocathode. These tracks decrease the average photocathode resistivity but also increase its non-uniformity by creating regions with different abilities to neutralise the charge left by the ejection of photoelectrons. Thus, depending on the rate, distribution and intensity of the incoming light pulses, the increase of the resistivity enhances the local charging of the photocathode which consequently attenuates and distorts the electric field of the input optics. In addition to the variation of the quantum efficiency (ϵ) [22], the consequences of this charging are an increase of the variance of the single photoelectron response and a decrease of the electron multiplication at the first dynode. The observed qualitative decrease in the mean response of the PMTs is consistent with the increase in the rate of energy deposited in the liquid xenon target volume from the ^{137}Cs and Am-Be sources and the consequent increase of the rate of scintillation photons arriving at the photocathodes.

Given the absence of dedicated calibration light sources in the ZEPLIN-III setup, searching for PMT signals corresponding to thermal single photoelectron emission ("dark counts") presents the only way to validate the calibration results obtained using the method described in Sec. 3. For this purpose, a dedicated data set was acquired with the DAQ triggering from an external pulser (100 Hz). The PMT signals were digitized at 2 ns sampling over a time segment of 256 μs starting at the trigger instant. The total duration of the run was about 60 hours which corresponds to about 500 s live time for each of the 31 PMTs. The raw data were reduced using a software threshold of $V_{thr} = 3\sigma$ (Eq. 5). For each PMT, the spectrum of the pulse amplitude was used to identify and eliminate the roughly exponential contribution of the noise just above V_{thr}. The surviving pulses were then assumed to be from thermal single electron emission from the PMT photocathodes provided that no coincident pulses were found in any of the other PMT channels. To exclude a connection to any possible interaction in the xenon target, the anticoincidence was expanded to all channels during a time window of 200 ns either side of the candidate pulse starting time. One can further assume that the area spectrum of the pulses corresponding to thermal photoelectrons is a good approximation‡ to the SER of a PMT, given that the probability of having $n > 1$ thermal photoelectrons ejected during a time window of $\lesssim 100$ ns is in fact very small. Fig. 6 shows the pulse area spectrum of thermal single photoelectron signals from the PMT also represented in Figs. 3 and 5. The average mean response of the PMTs to single photoelectron signals, characterized by the mean values of the area spectra, were found to differ by only $\approx 5.3\%$ from the values calculated using the method described in Sec. 3 using the WIMP-search data set. The average width of the PMTs SER, characterized by the *root mean square* of the area spectra, differs $\approx 15\%$ from the values estimated using Eq. 10 for the WIMP-search data set.

5. Conclusions

In the present work a method to calibrate the SER and assess the linearity of response of an array of PMTs is described. The method, which does not require dedicated runs, was applied to the science data from the ZEPLIN-III experiment. Excellent agreement were found when comparing the SER mean and width with those derived from a more traditional measurement using thermal photoelectron emission. Significantly, as the

‡ See [23, 18] for further details on reported differences between the spectra from thermal noise and PMT response to low intensity light pulses.

presented calculations rely only on the statistical description of the light pulses arriving at the PMTs photocathodes, the method is suitable to use with any array of photo detectors (e.g. PMTs, APDs, MPPCs) in applications ranging from low energy rare events searches to medical PET.

References

[1] Araujo H *et al. Astroparticle Physics* **26** 140
[2] Akimov D *et al.* 2007 *Astroparticle Physics* **27** 46 – 60
[3] Lebedenko V N *et al. In Press*
[4] Wright G T 1954 *J. Sci. Instrum.* **31** 377–381
[5] Breitenberger E 1955 *Prog. in Nucl. Phys.* **4** 56–94
[6] Lombard F J and Martin F 1961 *Rev. Sci. Inst.* **32-2** 200–201
[7] Delaney C F G and Walton P W 1964 *Nucl. Instr. Meth.* **25** 353–356
[8] Iinuma T A and Burch P R J 1962 *Nuclear Instruments and Methods* **16** 247 – 261
[9] Tusting R F, Kerns Q A and Knudsen H K 1962 *IEEE Transactions on Nuclear Science* **9** 118–223
[10] Prescott J R and Takhar P S 1962 *IEEE Trans. Nucl. Science* **9** 36–45
[11] Baldwin G C and Friedman S I 1965 *Review of Scientific Instruments* **36** 16–18
[12] GALE H J and GIBSON J A B 1966 *J. Sci. Iinstrum.* **43** 224–228
[13] Prescott J R 1966 *Nucl. Inst. Meth.* **39** 173–179
[14] Wright A G 1987 *IEEE Trans. Nucl. Sci.* **34(1)** 414–417
[15] Solovov V N *et al. In Preparation*
[16] Fried D L 1965 *Appl. Optics* **4** 79–80
[17] Morton G A 1968 *Appl. Opt.* **7** 1–10
[18] Dossi R, Ianni A, Ranucci G and Smirnov O J 2000 *Nucl. Instrum. Meth.* **A451** 623–637
[19] Press W H, Flannery B P, Teukolsky S A and Vetterling W T *Numerical recipes in C : The art of scientific computing* Cambridge University Press, 2002
[20] Araujo H M, Chepel V Y, Lopes M I, Van der Marel J, Ferreira Marques R and Policarpo A J P L 1998 *IEEE Trans. Nucl. Sci.* **45(3)** 542–548
[21] Murray R B and Manning J J 1960 *IRE Trans. Nucl. Sci.* **NS-7** 80–86
[22] Araujo H M *et al.* 2004 *Nucl. Instrum. Meth.* **A521** 407–415
[23] Candy B H 1985 *Review of Scientific Instruments* **56** 183–193

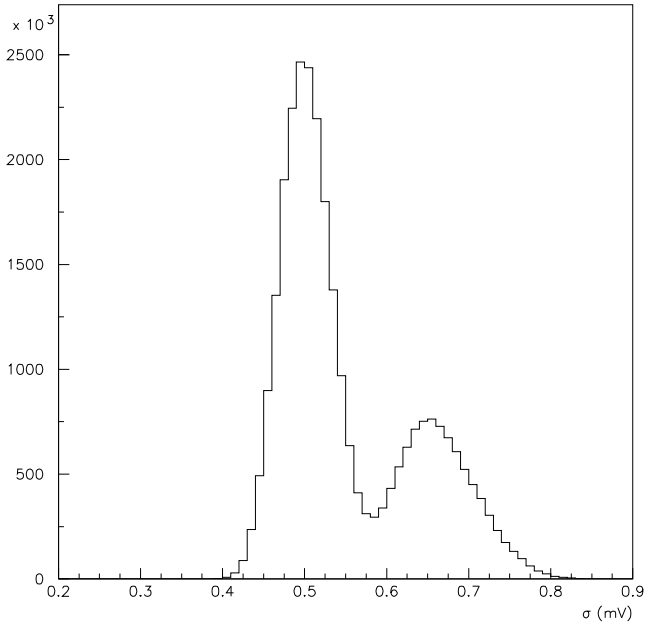

Figure 1. Distribution of values of σ (Eq. 4) for the central PMT in the ZEPLIN-III array.

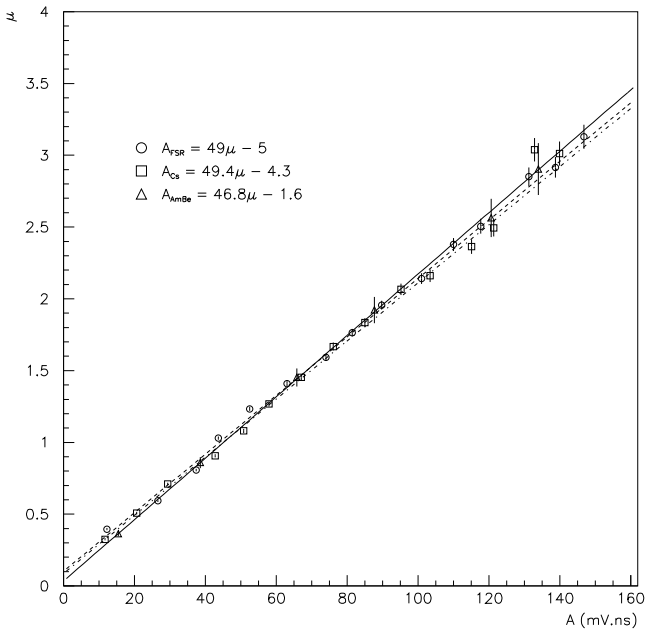

Figure 2. Calibration results for PMT 24 in the ZEPLIN-III array. The values of the $\mu(A)$ distributions and the corresponding linear fits are shown for: (squares) ^{137}Cs data set, (triangles) Am-Be data set and (circles) WIMP-search data set.

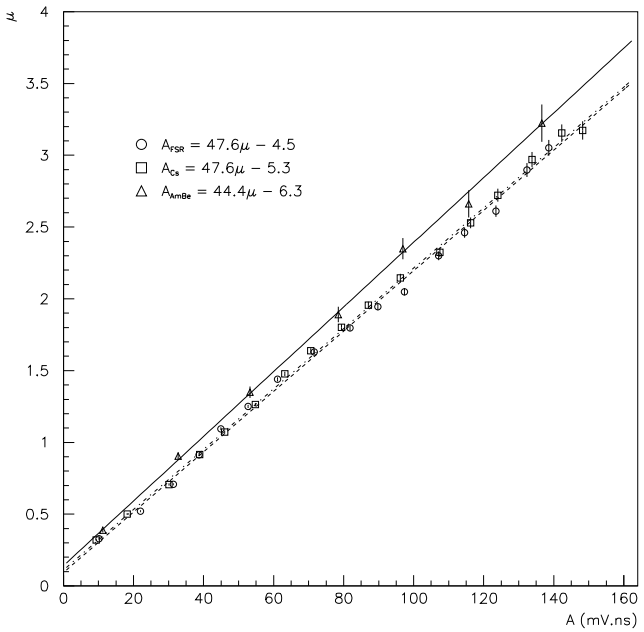

Figure 3. Calibration results for PMT 7 in the ZEPLIN-III array. The values of the $\mu(A)$ distributions and the corresponding linear fits are shown for: (squares) ^{137}Cs data set, (triangles) Am-Be data set and (circles) WIMP-search data set.

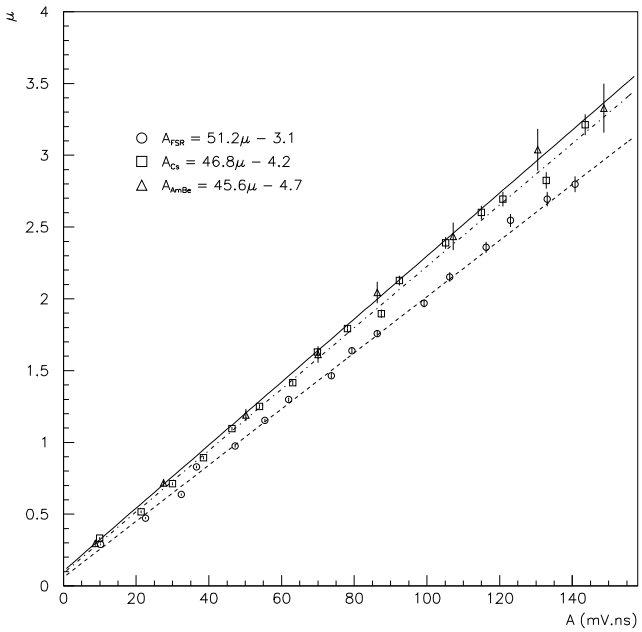

Figure 4. Calibration results for PMT 13 in the ZEPLIN-III array. The values of the $\mu(A)$ distributions and the corresponding linear fits are shown for: (squares) ^{137}Cs data set, (triangles) Am-Be data set and (circles) WIMP-search data set.

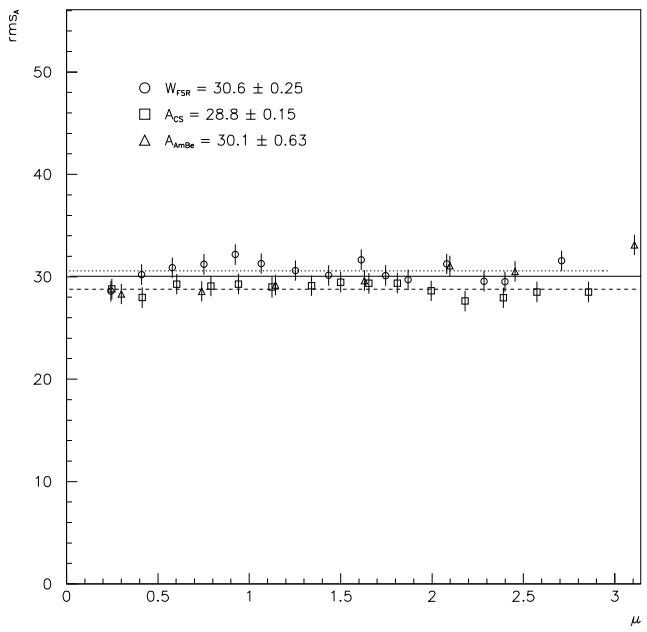

Figure 5. SER width results for PMT 7 in the ZEPLIN-III array. The values of $(\sigma_{\mathscr{R}} \equiv rms_A)_{V>V_{thr}}$ and the corresponding averages are shown for: (squares) ^{137}Cs data set, (triangles) Am-Be data set and (circles) WIMP-search data set.

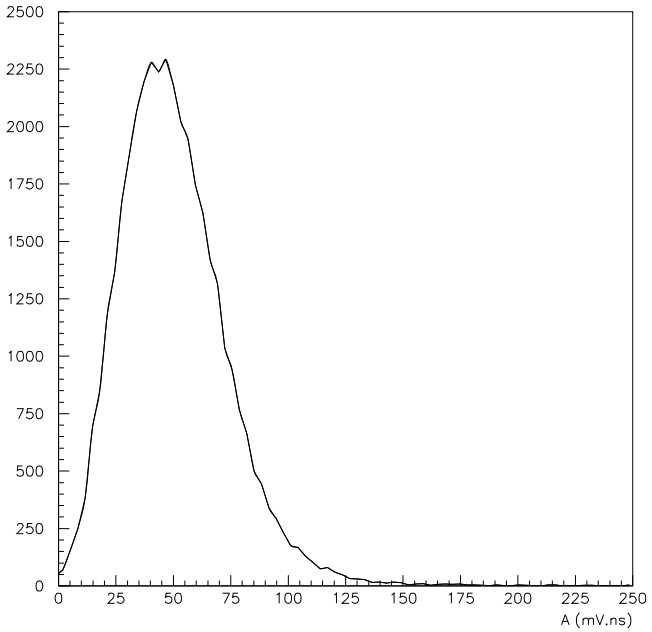

Figure 6. Pulse area spectrum of thermal single photoelectrons (for the same PMT also represented in Figs. 3 and 5).